Cucumber-Derived Exosome-like Nanovesicles Encapsulating Epigallocatechin Gallate for Skin Depigmentation: Molecular Docking, Stability, and Efficacy in B16/F10 Cells and Zebrafish

Li Tao [a,b,e], Ping Wang [a,b,e], Mengying Zhang [a,b,e], Wenyue Zhang [a,b], Rui Zhang [a,b], Junhao Tao [a,b], Mingyuan Chen [a,b], Jing Wu [c], Kawagishi Hirokazu [d], Peishi Feng [*a,b,e]

[a] *School of Pharmacy, Zhejiang University of Technology, Hangzhou 310014, China*

[b] *Zhejiang Provincial Key Laboratory of TCM for Innovative R & D and Digital Intelligent Manufacturing of TCM Great Health Products, Hangzhou 310014, China*

[c] *Faculty of Agriculture, Iwate University, Morioka, Iwate 020-8550, Japan*

[d] *Graduate School of Agriculture, Shizuoka University, Shizuoka 422-8529, Japan.*

[e] *Zhejiang International Scientific & Technological Cooperation Base of Development and Utilization of Natural Products, Zhejiang University of Technology, Hangzhou 310014, China.*

* *Corresponding author Peishi Feng , E-mail address: fengpeishi@zjut.edu.cn*

Supplementary data

Materials and methods

Isolation and Purification of CEVs

Fresh cucumbers acquired from the farmers' market in Liaocheng City of Shandong Province were sequentially washed with tap water, deionized water and pre-cooled PBS (0.01 M, pH 7.2). Following the peeling and dicing process, the tissues were disrupted in chilled PBS at 4:1 (w/w) in a high-speed tissue disruptor (BARBOSA, Germany) at 25,000 rpm for 30 seconds. The homogenate was then filtered through a 200 mesh nylon sieve. The filtrate was centrifuged twice, first at 1500 × g for 15 min at 4 °C to form a pellet for removal of large cellular debris; then at 6000 × g for 25 min. The resulting heavier pellet was collected at 10000 × g for 40 min. The supernatant was filtered through membranes 0.45 μm and 0.22 μm PES to check its sterility and remove larger particles.

An amount of PEG-6000 was added to give a final concentration of 10% (w/v) and kept at 4 °C for 16 h to induce vesicle aggregation and centrifuged at 8000 g for 30 min at 4 °C. After resuspending the pellet in PBS, the substance was centrifuged once more under similar circumstances (8,000 × g, 30 min) to remove residual contaminants. It ended up as a semi-purified CEVs suspension.

The suspension was dialyzed against glycine-Tris buffer (mass ratio 4.8:1, pH 8.3) using a regenerated cellulose membrane (300 kDa MWCO) under a constant current of 300 mA (Bio-Rad PowerPac™) for five 30-minute cycles, with buffer replacement between cycles. The sample was concentrated using a 100 kDa centrifugal ultrafiltration (Millipore, USA) unit at 4,000 × g for 20 min. The concentrated pellet was resuspended in 5 ml of PBS. The CEVs concentration was quantified using the BCA assay (PBeyotime Biotech-nology, China), and aliquots were stored at -80 °C for further use.

HPLC Analysis Conditions for EGCG

The mobile phase consisted of 0.1% (v/v) formic acid in water (solvent B) and acetonitrile (solvent A) under gradient elution conditions. The flow rate was maintained at 1.0 mL/min, the detection wavelength was set at 280 nm, and the injection volume was 7 μL. EGCG was identified based on its characteristic retention time (6.9 ± 0.1 min) and quantified using an external calibration curve exhibiting a correlation coefficient (R^2) greater than 0.999.

$$Y = 8475.6567 - 65.4457 \qquad R^2 = 0.9998$$

where Y is peak area and X is concentration (mg/mL).

Composition Analysis of CEVs

Sample Preparation

After thawing, the sample was thoroughly vortexed to ensure homogeneity. Subsequently, 200 μL of the thawed sample was combined with 500 μL of a 70% methanol aqueous solution containing an internal standard, and the mixture was vortexed continuously for 2 min to achieve complete extraction. The resulting mixture was rapidly frozen in liquid nitrogen for 5 min, thawed on ice for 5 min, and vortexed for 2 min to maintain consistency; this freezing-thawing-vortexing sequence was repeated 3 times. Afterward, the sample underwent centrifugation at 12,000 rpm for 10 minutes at 4 °C. The entire supernatant was isolated and concentrated to complete dryness. Upon reaching a dry state, it was reconstituted with 100 μL of a 70% methanol aqueous solution without an internal standard, vortexed for 3 minutes to ensure resuspension, and sonicated in an ice water bath for 10 minutes to optimize dissolution. This was followed by another centrifugation step at 12,000 rpm for 3 minutes at 4 °C. Finally, the clarified supernatant was transferred to an inner tube of an injection vial and stored for subsequent LC-MS/MS analysis.

UPLC-ESI-MS/MS Analysis

Chromatographic and mass spectrometric analysis was performed in configuration UPLC-ESI-MS/MS (exionlc ultra-performance liquid chromatography

system (https://sciex.com.cn/) and tandem mass spectrometry detector) on sample extracts. We utilized an Agilent SB-C18 column (1.8 μm particle size, 2.1 mm internal diameter × 100 mm length) as well as a mobile phase containing solvent A (pure water containing 0.1% formic acid) and solvent B (acetonitrile containing 0.1% formic acid). For the sample elution, a gradient method was used, starting with 95% solvent A and 5% solvent B, and after 9 minutes, the composition was linearly shifted to 5% solvent A and 95% solvent B and held for 1 minute. The solution was immediately increased to 95% solvent A and 5% solvent B for a total of 1.1 min, then maintained for a total of 2.9 min. The flow rate was 0.35 mL/min, column temperature was kept at 40 °C, injection volume was two μL, with column effluent being continuously interfaced to an ESI-triple quadrupole-linear ion trap (QTRAP)-MS for simultaneous detection.

The triple quadrupole mass spectrometer operated with an ESI source at 500 °C. The voltage used for ion spray was set to 5500 V (positive ion mode) and -4500 V (negative ion mode). Gas I (GSI) was maintained at 50 psi. Gas II (GSII) was regulated at 60 psi. The curtain gas (CUR) was regulated at a pressure of 25 psi. Dissociation of collision activation type was set to high. MRM scans were carried out using nitrogen as the collision gas at an intermediate pressure. The declustering potential (DP) and collision energy (CE) parameters were subsequently optimized for each MRM transition individually. In case of different elution ranges, monitoring was confined to only those MRM transitions of metabolites eluted at that timing.

Cellular uptake

PKH67 (2 μL) was diluted in 10 μL PBS to prepare the working solution. Then, 50 μL exosome suspension (CEVs or EGCG@CEVs) was incubated with PKH67 for 10 min at RT (room temperature) in the dark. Unbound dye was removed by centrifugation at 12,000 × g for 10 min using a 100 kDa filter.

B16F10 cells were seeded in 24-well plates in DMEM with 10% FBS. After reaching 60% confluence, cells were serum-starved overnight in FBS-free DMEM to

synchronize them. Labeled exosomes (CEVs-PKH67 or EGCG@CEVs-PKH67) were added and incubated at 37 °C with 5% CO_2 for 24 h.

Post-incubation, cells were washed with PBS, fixed with 4% paraformaldehyde for 15 min at RT, and permeabilized with 0.2% Triton X-100 for 10 min at RT. Then, cells were incubated with Alexa Fluor 488-phalloidin (2 drops/mL in PBS) for 30 min at 37 °C in the dark, followed by PBS washes.

After aspirating phalloidin, nuclei were stained with 1 μg/mL DAPI for 5 min. Excess DAPI was washed with PBS, and coverslips were mounted with antifade medium. Internalization of exosomes and the cytoskeleton was visualized by confocal microscopy (excitation/emission: 488/525 nm for PKH67, 405/461 nm for DAPI).

Network Pharmacology Analysis

Identification and Compilation of Targets for Potential Active Constituents in CEVs

The SMILES notations of the chemical constituents identified via UPLC-MS/MS analysis were retrieved from the PubChem database (https://pubchem.ncbi.nlm.nih.gov/) and submitted to the Swiss Target Prediction platform (http://www.swisstargetprediction.ch/) to predict potential biological targets. The Swiss Target Prediction platform uses molecular chemical structure, ligand similarity, cross-validation, and permutation analysis to predict targets for bioactive molecules. All target predictions were restricted to the model organism *Homo sapiens*

Screening of Targets of CEVs Against pigmentation

Pigmentation-associated targets were identified using the GeneCards (https://www.genecards.org/) and OMIM (https://omim.org/) databases. After removing duplicates and filtering, a list of pigmentation-related targets was compiled. GeneCards targets were filtered for precision using a relevance score ≥4.5. CEVs-associated targets were intersected with disease-related targets using Venny 2.1.0 (http://www.liuxiaoyuyuan.cn/). Overlapping targets were analyzed to identify those mediating the anti-pigmentation effects of CEVs. A drug component-gene network was constructed to depict the relationships between constituents and targets,

elucidating mechanisms of action. In Cytoscape 3.9.01, active components of CEVs and their potential therapeutic targets (intersecting targets) for pigmentation were incorporated. Nodes represented the components and target proteins. Topological analysis using the CytoNCA plugin identified key CEV components for anti-pigmentation based on node degree.

Investigation of Protein-Protein Interactions

Protein-protein interactions (PPIs) indicate associations between proteins. In tersecting genes were analyzed using the STRING database (https://cn.string-db.org/), with Homo sapiens as the organism and a confidence score ≥ 0.4; disco nnected nodes were excluded. The PPI network was visualized with Cytoscape 3.9.1. Topological parameters (closeness, degree and betweenness) were comput ed using the Centiscape plugin 2.2. Nodes were prioritized based on degree, id entifying the top 10 targets as core candidates for CEVs in pigmentation thera py. Biologically meaningful genes were identified with high parameter values, which simplifies the PPI network.

Gene Ontology (GO) and Kyoto Encyclopedia of Genes and Genomes (KEGG) Pathway Enrichment Analysis

Functional enrichment analyses using GO and KEGG pathways were cond ucted to delineate the molecular mechanisms underlying CEVs' anti-pigmentatio n activity. The analyses have linked potential targets with various biological pr ocesses and signalling pathways. Using DAVID (https://david.ncifcrf.gov/), the o verlapping genes were functionally annotated for their Molecular Functions (MF), Biological Processes (BP), Cellular Components (CC), and KEGG pathways.Th e bioinformatics platform (http://www.bioinformatics.com.cn/) was used to visual ize the results.

Molecular docking

Molecular docking was performed to analyze the binding affinity of the ac tive ingredients in CEVs with the target protein. Ligand 2D structures were ob

tained from PubChem (http://pubchem.ncbi.nlm.nih.gov/), converted to 3D using ChemOffice 20.0, and exported as MOL2 files. Protein crystal structures were obtained from the RCSB PDB (http://www.rcsb.org/) and preprocessed with Py MOL 2.6.0 to remove water and phosphate groups, saving the resulting structur es as PDB files. Ligand energy minimization, protein preprocessing, and bindin g pocket identification were performed using MOE 2019. Docking simulations were performed in MOE 2019 with 50 runs. Binding affinity was quantified us ing energy values: below -4.25 kcal/mol (moderate), -5.0 kcal/mol (good), and -7.0 kcal/mol (strong). Interactions and binding sites were visualized using PyM OL 2.6.0 and Discovery Studio 2019

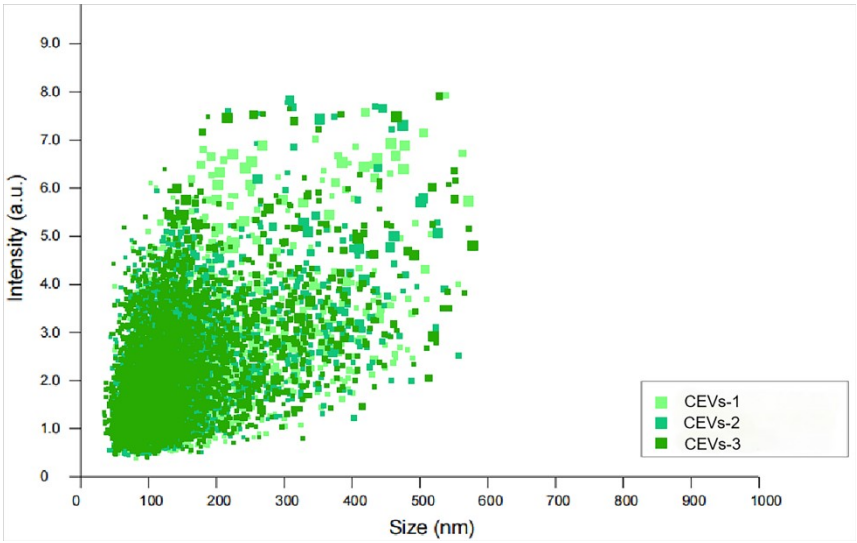

Fig. S0. Intensity/Size distribution from three replicate NTA measurements of CEVs

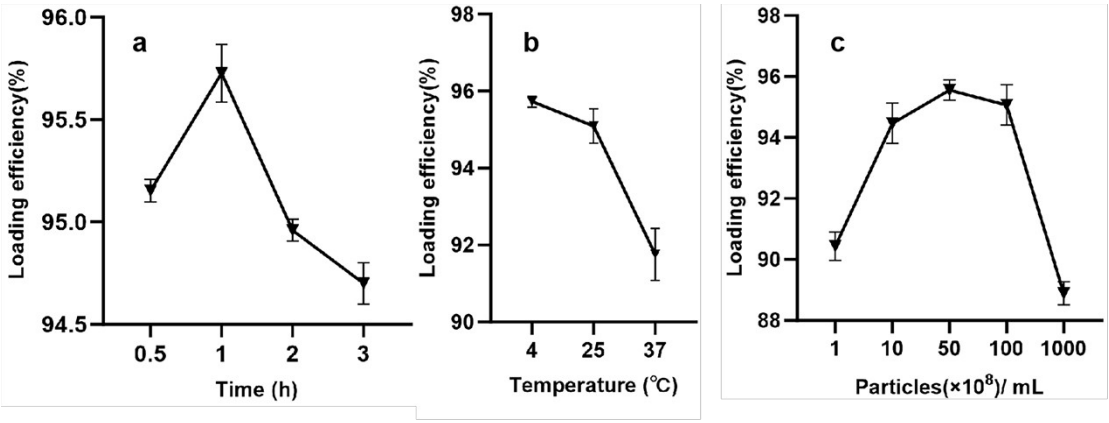

Fig. S1. Effects on loading efficiency: (a) time, (b) temperature, (c) concentration

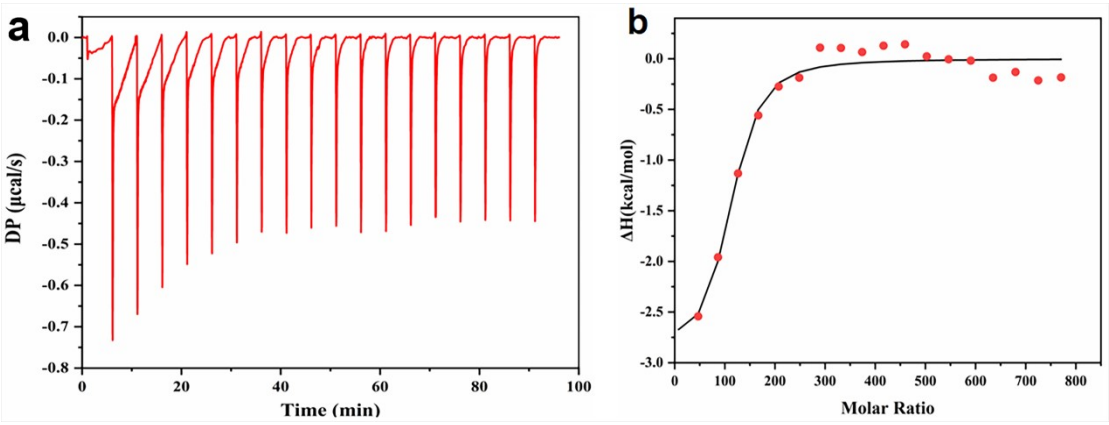

Fig. S2. Thermograms (a) and binding isotherms (b) corresponding to the titration of 4 mM EGCG with CEVs.

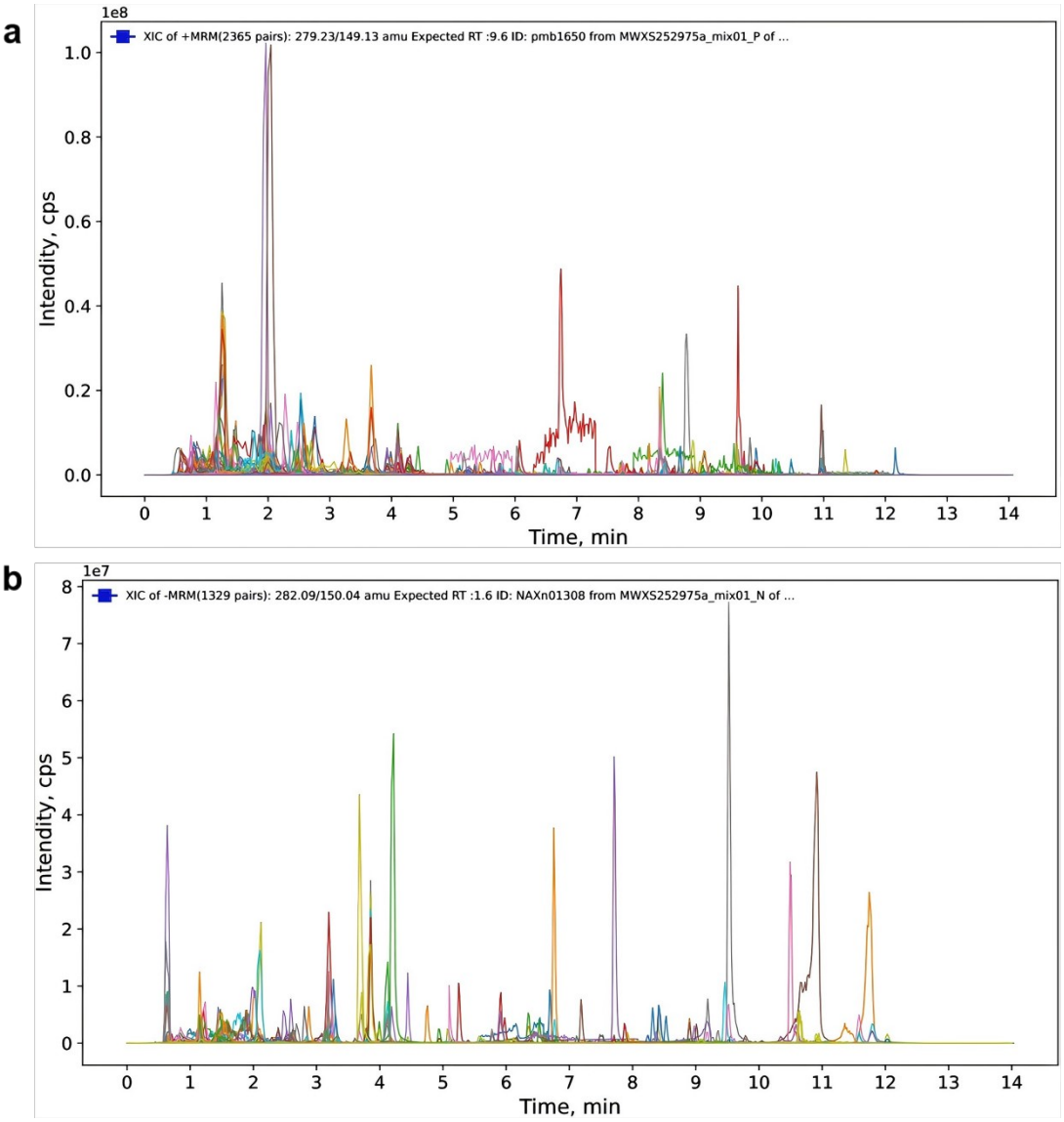

Fig. S3. Multi-peak plots of MRM metabolite detection in positive ion mode (a) and negative ion mode (b) mixed quality control (QC) samples.

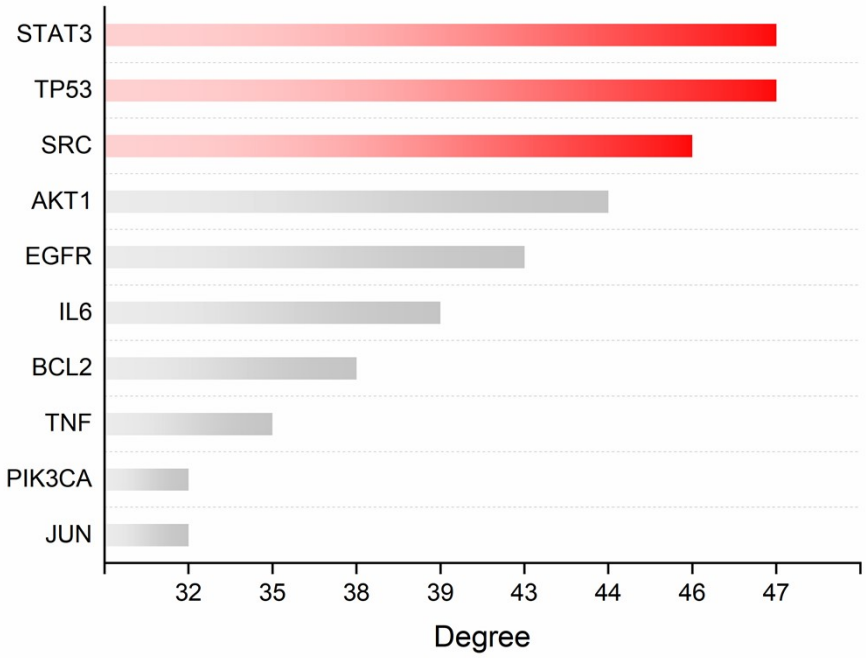

Fig. S4 Top 10 potential targets based on degree values

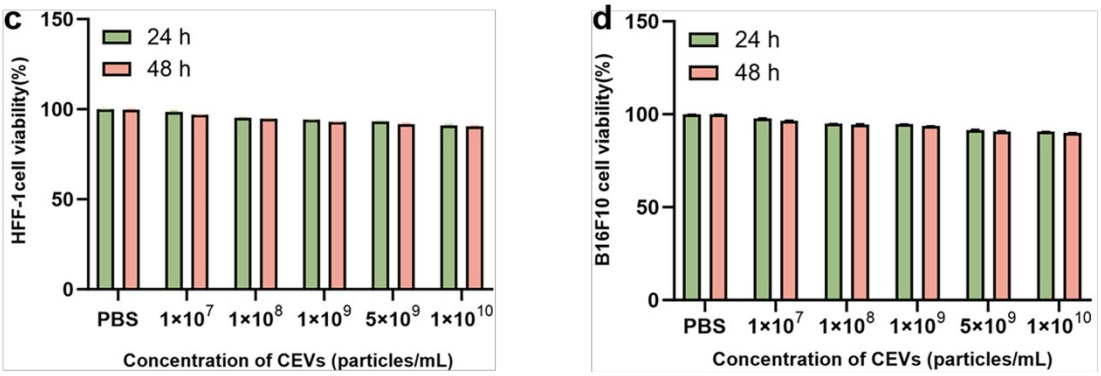

Fig. S5. The effect of CEVs on HFF-1 and B16F10 cell proliferation by CCK8 assay

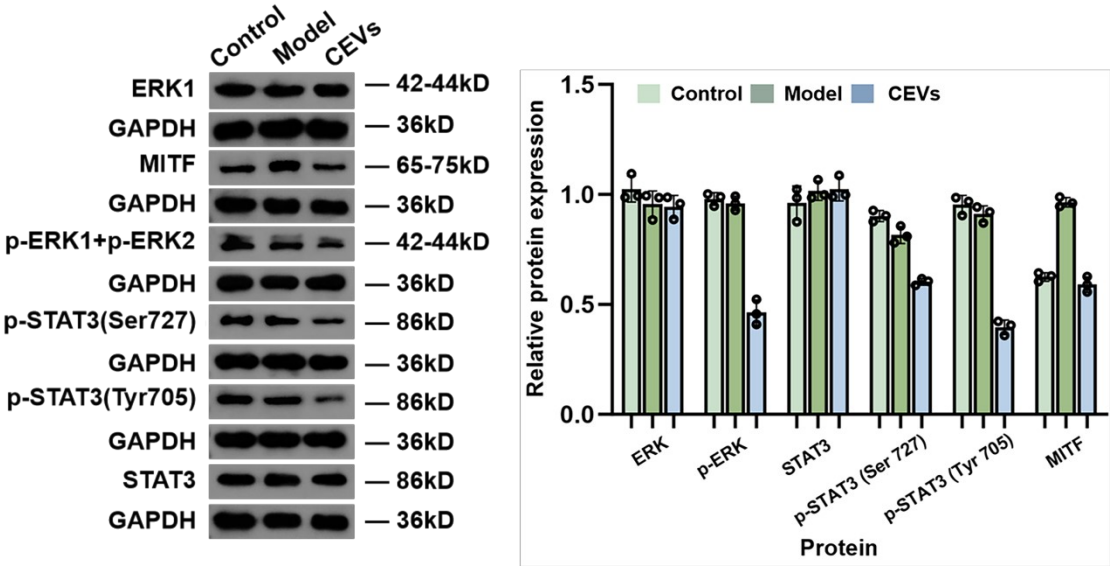

213

214 **Fig. S6.** The CEVs inhibits the α-MSH-induced activation of the ERK-STAT3-MITF
215 pathway. (a) Representative western blot images showing protein levels in the
216 validation experiment (Control, Model, and Treatment groups). (b) Quantitative
217 analysis of target proteins.

218

219

220

221

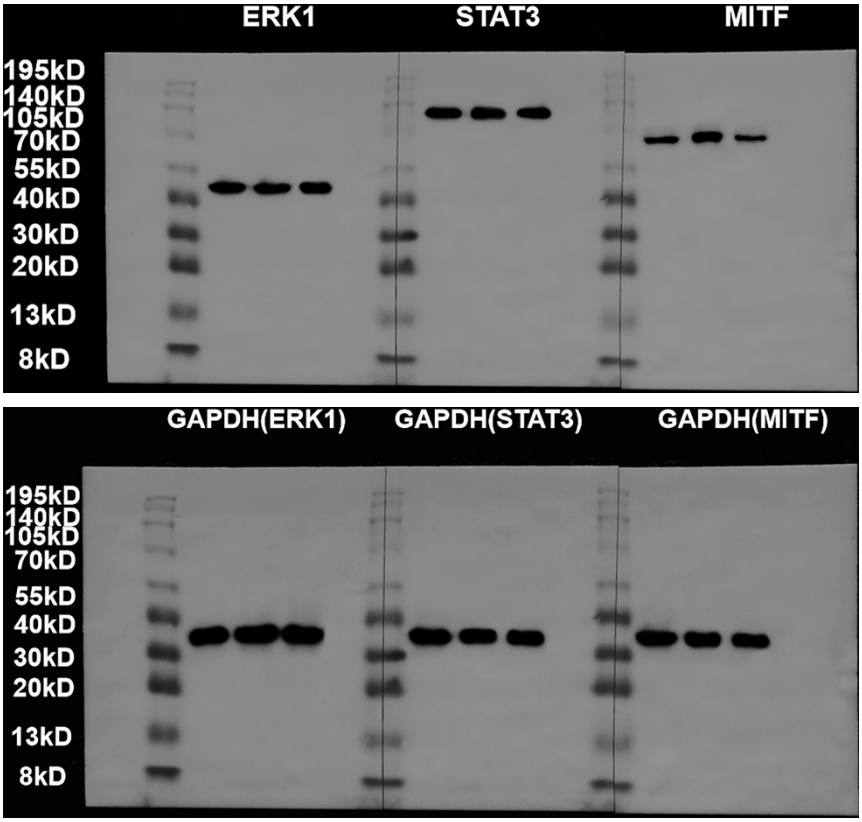

222

223

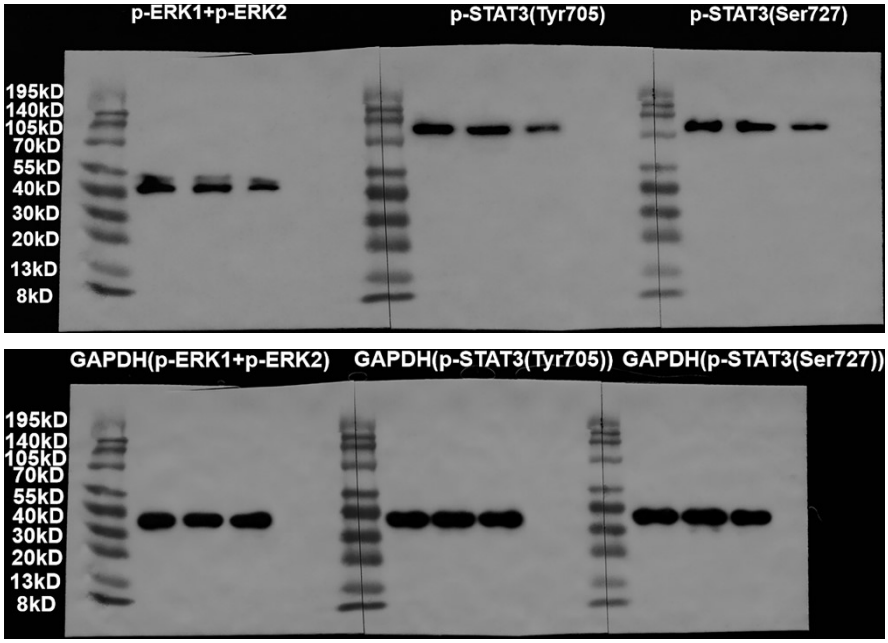

Fig. S7. Raw western blot data for Fig.S6

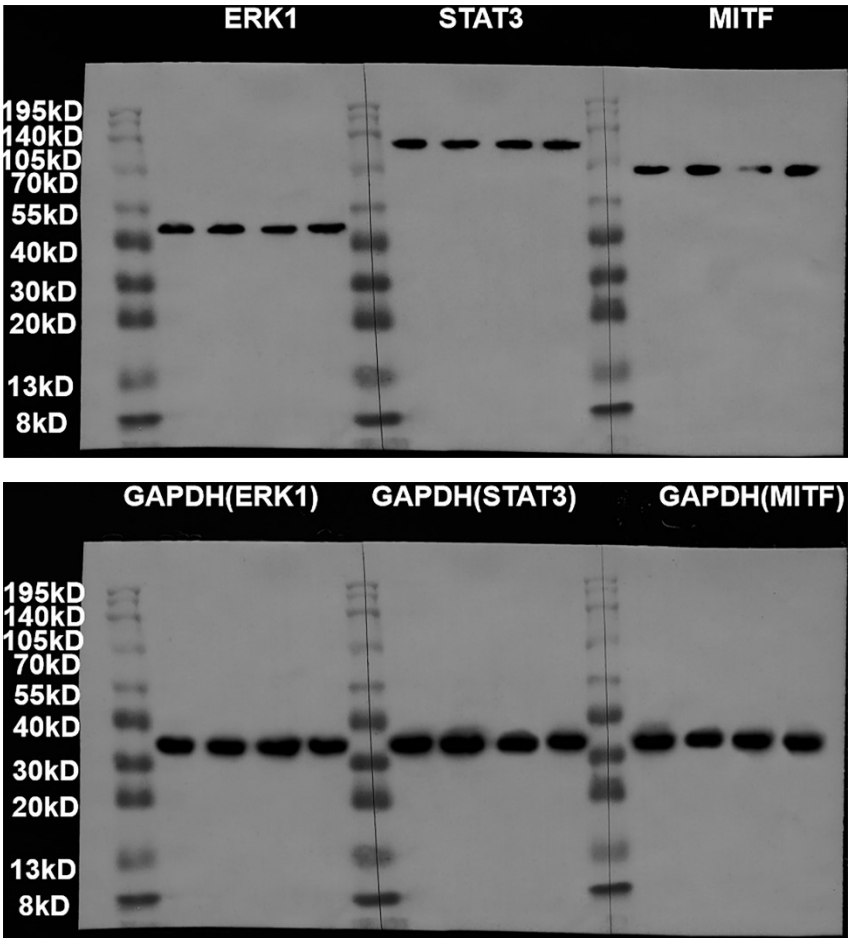

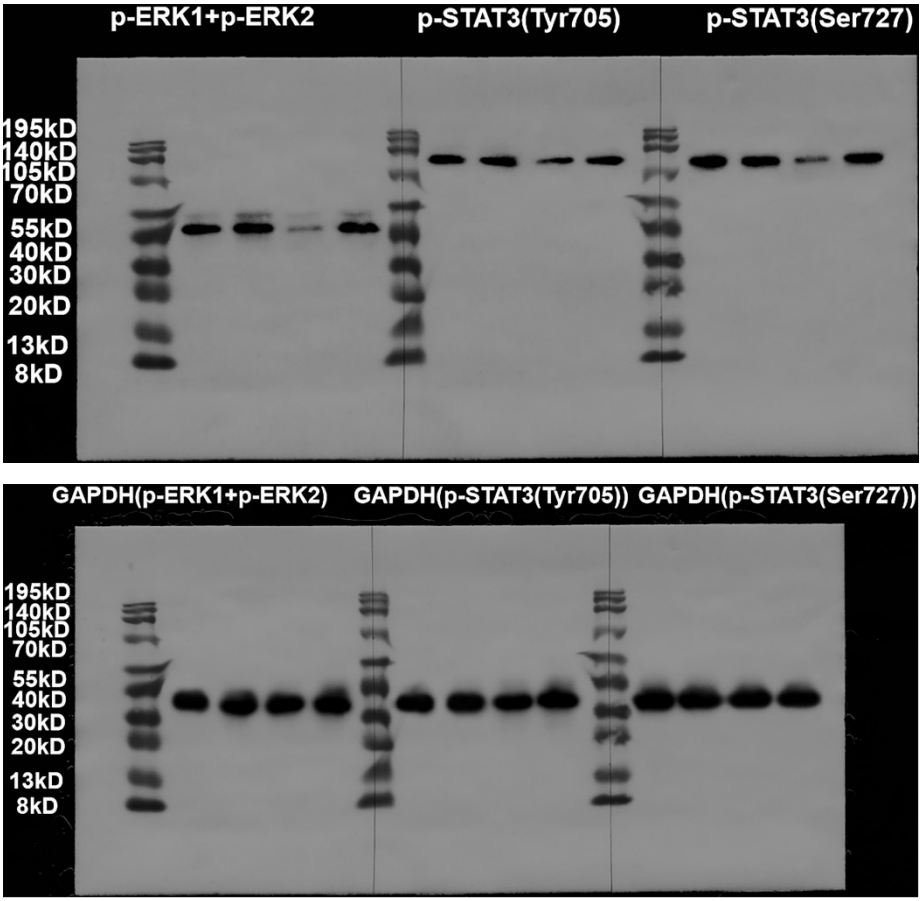

Fig. S7. Raw western blot data for Fig.9

Table S1 Thermodynamic parameters determined using ITC

	KD(M)	ΔH (kcal/mol)	ΔS (kcal/mol)	-TΔS (kcal/mol)
EGCG→CEVs	9.12e-6	-2.93	-6.88	-3.95

Table S2 Release Kinetic Models of EGCG from CEVs

Models	**Linear fitting($Q=M_t/M_{max}$)**	**R^2**
Zero-order kinetics	$Q \sim t$	0.9368
First-order kinetics	$-\ln(1-Q) \sim t$	0.9537
Higuchi model	$Q \sim t^{0.5}$	0.9673
Korsmeyer-Peppas	$Q \sim t^n$	0.9654， n = 0.7231

Table S3 Representative Compounds from the Top 400 for Hyperpigmentation Therapy

Number	Compounds	Formula	CEVs
1	(2S)-2-(methylamino)pentanoic acid	C6H13NO2	182664546.2
2	2-Decanol*	C10H22O	157311928.8
3	1-Decanol*	C10H22O	150175452
4	cis,cis-Muconate*	C6H6O4	99688778.47
5	2-[[2-amino-3-(4-hydroxyphenyl)propanoyl]amino]-3-methylpentanoic acid	C15H22N2O4	77766701.97
6	2-Methylpyrrolidine-2-carboxylic acid*	C6H11NO2	72387679.89
7	4-methoxybenzamide	C8H9NO2	69295024.76
8	Lidocaine	C14H22N2O	68149574.7
9	(5R)-5-(methylaminomethyl)oxolan-2-one*	C6H11NO2	65288419.93
10	2-Oxo-2,3-dihydrofuran-5-acetate*	C6H6O4	54937204.93
11	(2R,4R)-4-methylpyrrolidine-2-carboxylic acid	C6H11NO2	47313022.81
12	4-Methylazetidine-2-Carboxylic acid	C5H9NO2	45346385.85
13	13-(methoxymethyl)-10,11,11-trimethyltetracyclo[8.2.1.01,5.08,12]tridec-6-en-13-ol	C18H28O2	45072406.95
14	8-Hydroxyquinoline	C9H7NO	42615912.79
15	(2R)-5-oxooxolane-2-carboxamide	C5H7NO3	33024080.53
16	Choline	C5H14NO+	29602219.14
17	Indole-4-Carboxaldehyde*	C9H7NO	29446611.97
18	L-Pipecolate	C6H11NO2	28169923.23

19	Piperidine	C5H11N	26082147.56
20	2-n-Propyl-3-pentenoic acid	C8H14O2	24177948.7
21	2-n-Propyl-4-pentenoic acid	C8H14O2	23440263.74
22	Embelin	C17H26O4	22203061.57
23	Dillapiole	C12H14O4	21836619.84
24	furo[2,3-h]quinoline	C11H7NO	21792433.65
25	6-Deoxyfagomine	C6H13NO2	21382210.05
26	Arcapillin	C18H16O8	20032094.47
27	2-Phenylpropylamine*	C9H13N	19600173.6
28	N-(3-hydroxy-4-methoxyphenethyl)-4-hydroxybutanamide	C14H21NO4	19564454.2
29	Amphetamine*	C9H13N	18875814.71
30	Dextropimaric acid	C18H28O2	15506125.66
31	isoemodin	C15H10O5	15297373.36
32	Emodin	C15H10O5	14404640.72
33	3-Chloroaniline	C6H6ClN	13629690.16
34	Lumichrome	C12H10N4O2	13504973.61
35	(1R,2S,4S)-6-methoxy-4,7-dimethyl-1-(propan-2-yl)-1,2,3,4-tetrahydronaphthalen-2-yl acetate	C18H26O3	13009809.7
36	Lamprolobine	C15H24N2O2	12798655.9
37	3-Hydroxylup-20(29)-en-28-al (Betulinaldehyde)	C30H48O2	12395055.07
38	N-Acetylindole-3-carboxaldehyde*	C11H9NO2	11984436.82
39	Trisporic Acid A	C18H26O3	11841407.56
40	4',5,6,7-Tetramethoxyflavanone	C19H20O6	11632449.87
41	Succinate*	C4H6O4	11604457.93
42	Tetradecyldiethanolamine	C18H39NO2	11332243.42
43	Podocarp-7-en-3-one*	C17H26O	10779765.01
44	Octadec-2-enamide*	C18H35NO	10764264.28
45	Octadec-8-enamide*	C18H35NO	10689527.16
46	Spermine	C10H26N4	10606433.15
47	Isoquinoline	C9H7N	10130865.13
48	17beta-Hydroxy-2alpha-(methoxymethyl)-17-methyl-5alpha-androstan-3-one	C22H36O3	10099817.32
49	1-aminobenzocyclobutene	C8H9N	9848515.772
50	4-Hydroxybenzaldehyde	C7H6O2	9597369.832
51	ethylbis(3-phenylpropyl)amine	C20H27N	8996161.213
52	(5S)-5-methyl-5-[(1S)-4-methylcyclohex-3-en-1-yl]oxolan-2-one	C12H18O2	8877289.356
53	Methylmalonate*	C4H6O4	8770915.194
54	2,2-dimethylchromene-6-carboxylic acid*	C12H12O3	8571228.289
55	2-(hydroxymethyl)-5-{4-imino-3h-furo[3,2-	C11H13N3O5	8483840.879

	d]pyrimidin-7-yl}oxolane-3,4-diol		
56	6-Pentadecylsalicylic acid	C22H36O3	8466191.882
57	3,4-dihydroxy phenylethanol	C8H10O3	8252296.013
58	4-Nitrophenol	C6H5NO3	8161880.433
59	Pyrrolidin	C4H9N	7833950.86
60	AMP*	C10H14N5O7P	7803247.736
61	7,8-dihydropterin*	C6H7N5O	7793293.292
62	Glycyroside*	C27H30O13	7618282.592
63	Podocarp-8-en-15-ol	C17H28O	7590182.815
64	Retronecine	C8H13NO2	7471354.011
65	7-(4-Hydroxyphenyl)-1-phenyl-4-hepten-3-one	C19H20O2	7463950.36
66	2-Phosphoglycolate	C2H5O6P	7284769.853
67	6-hydroxy-5-[(3E)-5-hydroxy-3-methylpent-3-en-1-yl]-1,1,4a,6-tetramethyl-decahydronaphthalen-2-yl acetate	C22H38O4	7019581.196
68	2-Amino-2-methylpropanoate	C4H9NO2	7018504.141
69	Quinoline	C9H7N	6961024.057
70	Diisobutyl phthalate*	C16H22O4	6946504.205
71	Indoline	C8H9N	6816286.604
72	2-amino-2-(1-methyl-1H-pyrazol-4-yl)acetic acid	C6H9N3O2	6775181.313
73	polygodial*	C15H22O2	6432403.196
74	13-Hydroxygermacrone*	C15H22O2	6350593.709
75	Benzoate	C7H6O2	6314128.429
76	Formononetin-7-O-β-D-Apiofuranosyl-(1→6)-β-D-Glucopyranoside	C27H30O13	5973233.813
77	3,7,11-trimethyl-2-oxa-6,10,13-triazatricyclo[7.3.1.05,13]tridecane	C12H23N3O	5786848.222
78	Vanillylamine	C8H11NO2	5693285.639
79	3,5-Di-tert-butylbenzoic acid	C15H22O2	5554468.507
80	3',4',5'-O-Trimethyltricetin	C18H16O7	5379497.071
81	Tetradecasphinganine	C14H31NO2	5321807.597
82	Dihydrobungeanool	C18H31NO2	5287637.493
83	Benzimidazole	C7H6N2	5271578.811
84	4-amino-2-methylbutanoic acid	C5H11NO2	5255335.52
85	Agmatine	C5H14N4	5171921.906
86	13-Methyl-8,11,13-Podocarpatriene-2,3-diol	C18H26O2	5117737.944
87	dasyscyphin A	C22H36O4	5065653.52
88	Cyclohexaneacetic acid	C8H14O2	5031125.285
89	Dodecanamide	C12H25NO	4957887.01
90	Turanose	C12H22O11	4768149.08
91	11-HpODE	C18H32O4	4694278.575

92	N-Methylnicotinate	C7H7NO2	4628901.149
93	N-[2-(3-indolyl)ethyl]succinamic acid	C14H16N2O3	4546020.265
94	Histamine	C5H9N3	4225068.886
95	N1-Methyl-2-pyridone-5-carboxamide	C7H8N2O2	4176635.158
96	cis-Aconitate	C6H6O6	4063689.151
97	Chrysophanic acid 9-anthrone	C15H12O3	3909816.099
98	1-Methylnicotinamide	C7H9N2O	3831332.734
99	Indole-3-carboxylate	C9H7NO2	3725739.147
100	Indole-5-carboxylic acid	C9H7NO2	3649342.601
101	2',4'-Dimethylacetophenone	C10H12O	3581486.465
102	Indole-3-carboxaldehyde	C9H7NO	3559580.731
103	Isobutyryl carnitine	C11H21NO4	3542594.711
104	D-Gluconic acid	C6H12O7	3504682.112
105	Ajaconine	C22H33NO3	3494011.578

*: There are isomers present in this substance.

Table S4 Information of top 10 Active Components From CEVs

Number	Compounds	Formula	CAS	Structure
1	4',5,6,7-Tetramethoxyflavanone	C19H20O6	2569-77-9	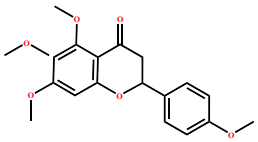
2	3',4',5'-O-Trimethyltricetin	C18H16O7	18103-42-9	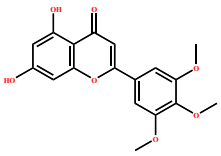
3	Dihydrobungeanool	C18H31NO2	-	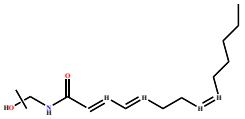
4	Arcapillin	C18H16O8	83162-82-7	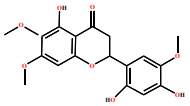
5	Embelin	C17H26O4	550-24-3	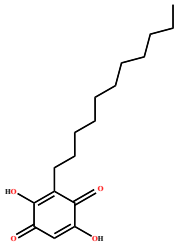

6	Emodin	C15H10O5	518-82-1	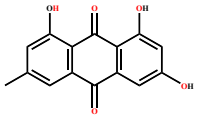
7	isoemodin	C15H10O5	-	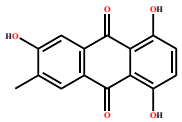
8	Dodecanamide	C12H25NO	-	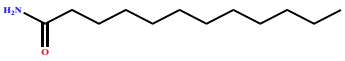
9	Glycyroside	C27H30O13	125310-04-5	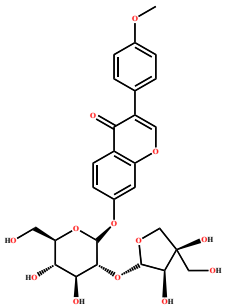
10	Isobutyryl carnitine	C11H21NO4	25518-49-4	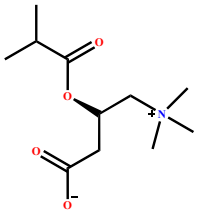

Table S5 Evaluation of Key Topological Parameters in the Protein-Protein Interaction Network. (the top 10 Degrees)

Rank	Name	Betweenness	Closeness	Degree
1	STAT3	0.05543660253705654	0.6518518518518518	47
2	TP53	0.15337835382552095	0.6666666666666666	47
3	SRC	0.07034453302411396	0.6470588235294118	46
4	AKT1	0.047189220643756656	0.6285714285714286	44
5	EGFR	0.06649664076977446	0.6285714285714286	43
6	IL6	0.03690167662309724	0.6153846153846154	39
7	BCL2	0.058564962620918884	0.6027397260273972	38
8	TNF	0.051546890192323565	0.5789473684210527	35
9	PIK3CA	0.0278343970798876	0.5605095541401274	32
10	JUN	0.018148358887829875	0.5789473684210527	32

Table S6 Docking Analysis of the Top 10 Active Ligands with Core Receptor Targets

Active Compounds	Docking Score (kcal/mol)
4',5,6,7-Tetramethoxyflavanone	-6.04
3',4',5'-O-Trimethyltricetin	-6.18
Dihydrobungeanool	-6.76
Arcapillin	-5.79
Embelin	-6.64
Emodin	-5.51
isoemodin	-5.41
Dodecanamide	-6.07
Glycyroside	-7.53
Isobutyryl carnitine	-5.99